공학석사 학위논문

Modeling charge transport in organic hosts: BCP and NBPhen

유기 호스트 물질인 BCP와 NBPhen 분자의 전하 거동 모델링

2020년 2월

서울대학교 대학원

재료공학부

조 재 영

Abstract

Modeling charge transport in organic hosts: BCP and NBPhen

Jaeyoung Cho
Department of Materials Science and Engineering
College of Engineering
Seoul National University

The charge carrier mobility of BCP and NBPhen which are commonly used as an electron transport material, are different from each other. Specifically, experimentally measured electron mobility of NBPhen is nearly 10 times larger than that of BCP and 9 times larger in charge carrier transport simulation. In order to unveil the relation between mobility and molecular structure, microscopic simulation method was used. In this methodology, amorphous system was constructed by using Molecular Dynamics (MD) simulation and electronic properties of molecule such as transfer integral, site energy of each molecular site and reorganization energy were calculated by using DFT method and Polarizable force field. Finally, charge dynamics was explicitly simulated by using Kinetic Monte Carlo method in the simulation box. The reason of difference in mobility can be categorized into three terms: energetic disorder, transfer integral and reorganization energy term. In the respective of energetic

disorder, larger molecular dipole distribution of NBPhen which results in high energetic disorder has negative effect on charge carrier mobility. However, in the respective of transfer integral and reorganization energy, higher average value of transfer integral and smaller value of reorganization energy of NBPhen have positive effect on charge carrier mobility, which exceed the negative effect from energetic disorder. This result is originated from the difference in molecular structure between BCP and NBPhen. To sum up, from this research, we only analyzed the difference between BCP and NBPhen molecule that have Phenanthroline core in common and difference in substituents. However, by analyzing the mobility difference with different substituent groups, the analysis of this research can be generalized. Furthermore, in order to obtain high mobility value, the molecule should be designed to have low energetic disorder and reorganization value, and high average value of transfer integral which can be achieved by analyzing the difference in electronic properties of molecules with different substituent and collective property of amorphous system.

Keywords: charge carrier mobility, BCP, NBPhen, microscopic simulation, MD simulation, transfer integral, site energy, reorganization energy, DFT, Kinetic Monte Carlo, energetic disorder, molecular dipole distribution
Student Number: 2018-27549

Contents

List of Tables

List of Figures

Chapter 1

Introduction

1.1 OLEDs

Organic light-emitting diodes (OLEDs) are one of the most wide spread and commercially successful example of organic electronics industry nowadays, which are used significantly in the high-end smartphone displays or cutting-edge large screen smart TV displays. It has advantages for using as displays and lightings due to its low cost of fabrication, lightweight, flexible property and superior color quality than that of traditional LEDs. However, there are still unsolved major problems in OLEDs industry such as color quality issues, efficiency issues and finally long-term stability issues[1] especially in blue OLEDs. An OLED device has one or multiple organic layers that are sandwiched between two electrodes with transparency. In single layer devices, hole and electron concentration will be imbalanced due to their different value in mobilities, which results in low efficiency.

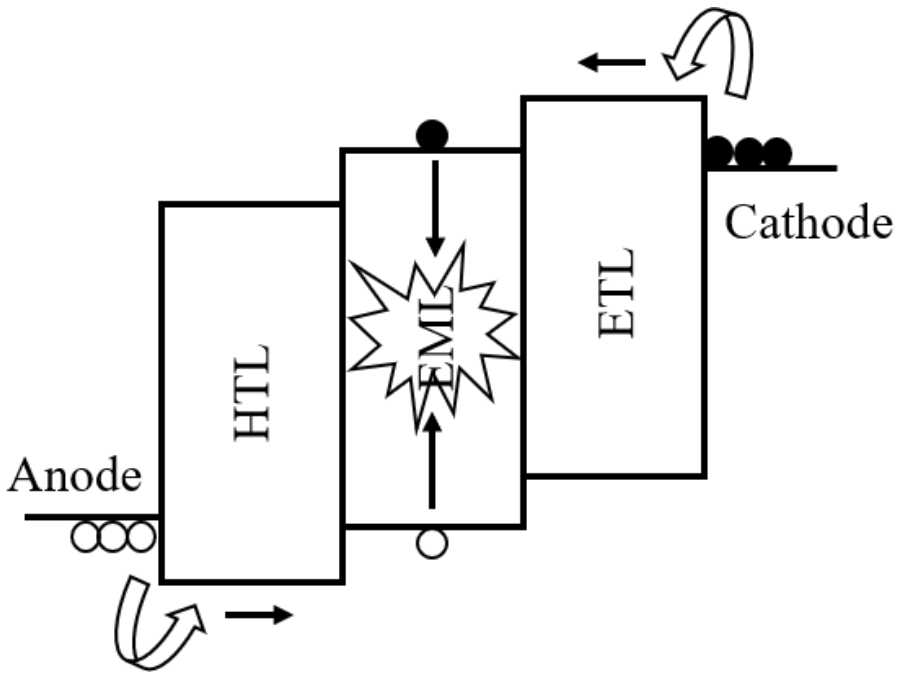

Figure 1.1 Schematic illustration of the working principle of OLED device. The holes and electrons flow from the HTL to EML and ETL to EML respectively. In the EML, recombination occurs to form excitons, which they decay to emit light radiatively.

Consequently, additional layers are added to the device in order to obtain higher efficiency which consists of an electron transport layer (ETL), a hole transport layer (HTL) and an emissive layer (EML). When the voltage is applied through the device, the injected carrier (electron and hole respectively from cathode and anode) flow from the ETL/HTL to the EML, where they meet and recombine with each other to form excitons.

Finally, the excitons generated from EML emit light through electroluminescence phenomenon. Additionally, often electron, hole or exciton blocking layers are used to prevent carriers or excitons from moving into the ETL/HTL and confine them to the EML, ensuring that they recombine.

1.2 Charge transfer theory

In organic semiconductor devices including OLEDs, charge transport can be described as ′hopping process′ between molecular sites. Hopping transport was introduced in impurity conduction in inorganic solid-state materials by Conwell[2] and Mott[3] in 1956. Compare to the regular

semiconductors, the conductivity increased with temperature which led to the conclusion that charge transport can be described by a series of discrete hops that are thermally activated. The same behavior was found in molecular semiconductors by Holstein[4,5] in 1959. He developed a model for charge transport in molecular crystals based on the ′localization of charges on molecular sites′. On each molecular sites, the electron is localized in the lowest occupied molecular orbital (LUMO) and will hop to the LUMO of an neighboring molecule. Along the same lines, the hole is localized in the highest occupied molecular orbital (HOMO) and will hop to the HOMO of an adjacent molecule. This spatially localized property of electronic states derived from the different nature of the bonding. In comparison to covalently bonded materials, organic molecules interact with each other via weaker Coulomb forces and Van der Waals forces. And due to the localization, sufficient electronic coupling between organic molecules is needed to allow for charge transport which can be achieved by π-systems formed by the p_z orbitals of sp^2-hybridized C-atoms.

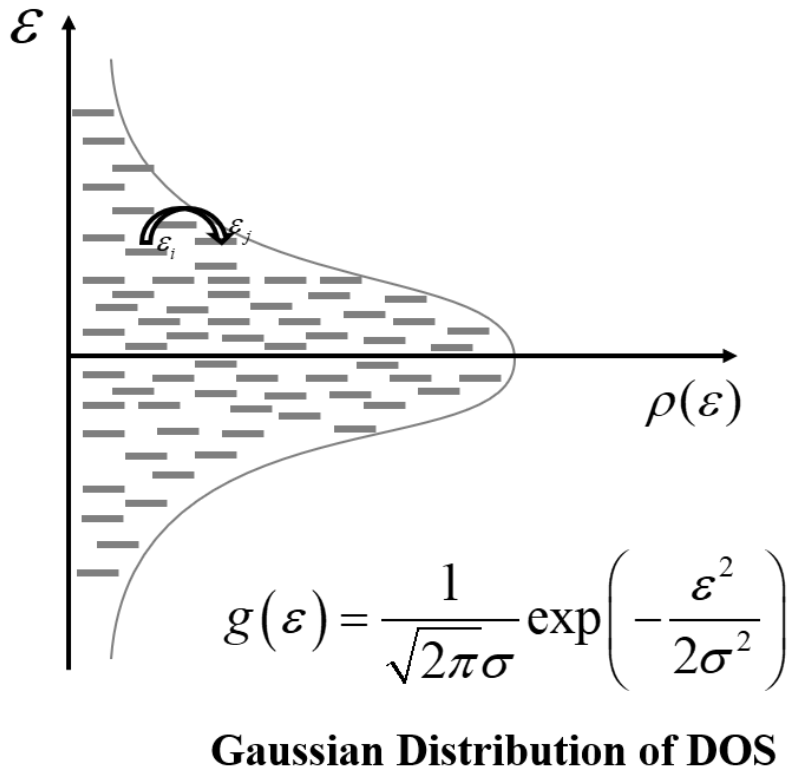

Figure 1.2 Schematic description of a Gaussian density of states in disordered organic semiconductors. Electrons and holes occupy the LUMO and HOMO energy levels of the molecules respectively.

1.3 Brief history of charge transport simulation

1.3.1 Lattice Model

The practical methodology for simulating charge transport simulation in organic semiconductors starts from the Bassler's work in 1993. He used the first 3D Monte Carlo (MC) simulation method to describe the hopping of a single carrier (electron or hole) on a cubic lattice system. The hopping rates between different lattice sites were calculated by Miller-Abrahams hopping rate equation[6], where the energies of each lattice sites were extracted from a Gaussian distribution with average m and standard deviation σ which describes the energetic disorder of amorphous system. This has led to the birth of the Gaussian Disorder Model (GDM)[7] and from this work we can obtain the field and temperature dependence of the charge carrier mobility in the nearly zero carrier concentration limit.

After the Bassler's research, it seemed that this GDM model could explain the hopping transport mechanism of charge carrier in organic semiconductors well. However, as pointed out by Gartstein and Conwell, who cast the doubts on limited Pool-Frenkel behavior[8] in a short field range, a spatially correlated potential for the charge carriers

was needed to explain the Poole-Frenkel behavior in a wide range of electric field. This model, which is called Correlated Disorder Model (CDM)[9] explains the cause for the correlation between site energies as charge-dipole interactions or thermal fluctuations in molecular geometries.

Even though CDM model could explain Poole Frenkel behavior in a wider range of electric field, it was realized that the importance of another parameter had been ignored in explaining the charge transport behavior in organic semiconductors: the charge carrier density. In 2005, Pasveer et al. showed the compact equations for temperature, electric field, and the charge carrier density dependence of the mobility from conjugated polymer single-carrier devices which is called the extended Gaussian disorder model (EGDM)[10]. Furthermore, an analogous approach was used for the case with spatial correlated disorder, which is called the extended correlated disorder model (ECDM)[11]. Nowadays, there are numerous kinds of OLED simulation program tools based on both EGDM and ECDM model available.

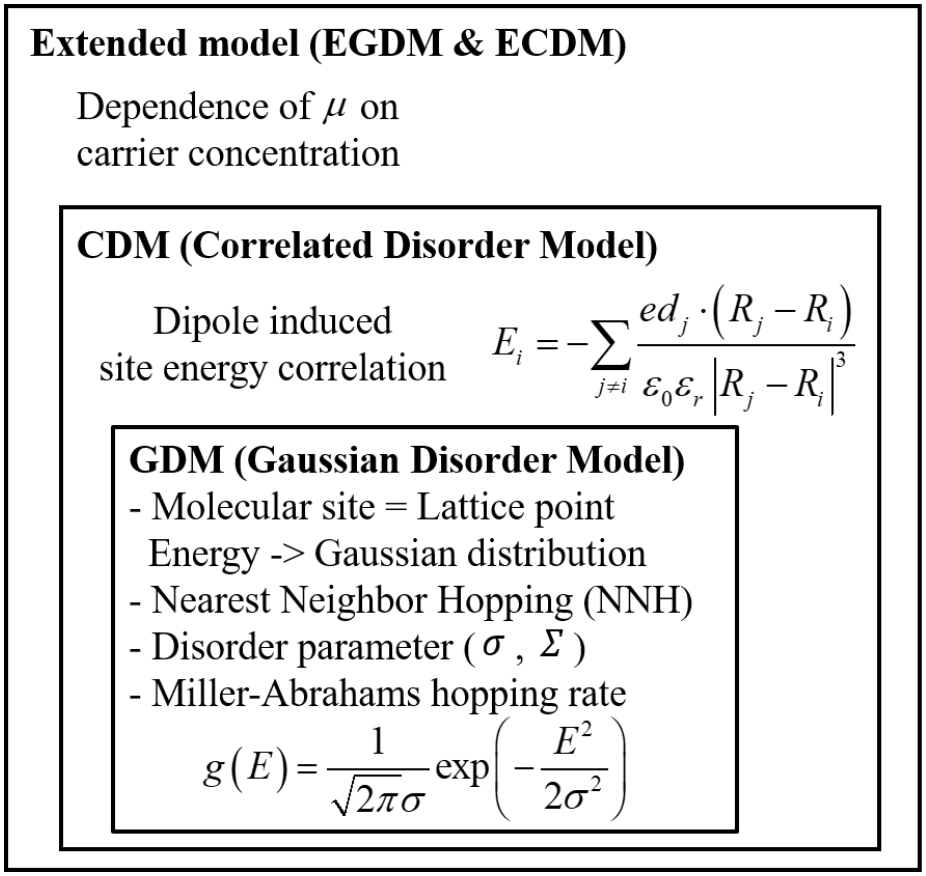

Figure 1.3 Schematic representation of the development of Lattice model simulation methodologies.

1.3.2 Microscopic Model

The fact that carrier transport in disordered OLEDs occurs via hopping process can be simulated by using computational modeling. The first step is to determine the structure of the molecules that composes the materials of each OLED layer, and the interaction between the molecules. Second, determine the morphology of the amorphous system which consists of organic small molecules by ab initio methods where the deposition of layers of the device is simulated by a Monte Carlo (MC)[12] or Molecular Dynamics (MD) simulation method[13]. The third step is determining hopping rates between molecular sites for all neighboring pairs. All these hopping rates can be obtained by calculating transfer integral for each pair of molecules in a system of the morphology and reorganization energy for specific molecule, for example using density functional theory (DFT). With the system morphology and hopping rates for every molecular pair at hand, we can simulate the charge transport process using stochastic simulation methods like Kinetic Monte Carlo (KMC)[14] or by constructing a system of equations for all transfer rates, called Master Equation (ME), and solving this equation in numerical manner[15]. Through this process, we can obtain the macroscopic property such as charge carrier mobility or diffusivity and such a modeling

approach which covers from atomic-scale to device-scale is referred to as ‘Multi-scale modeling’[16].

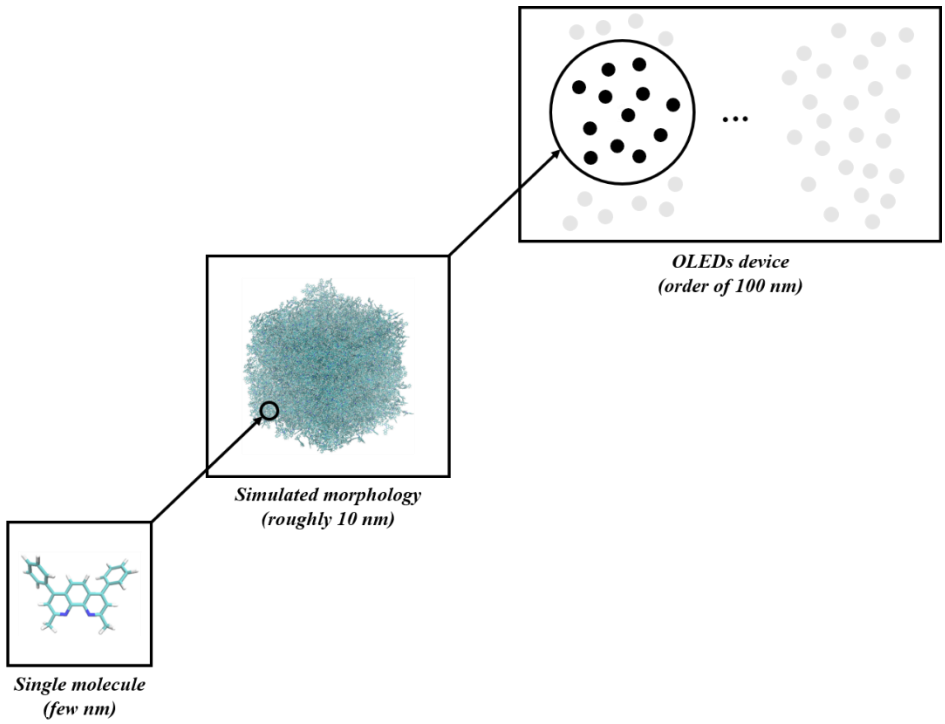

Figure 1.4 Schematic representation of the different length scales treated from the multi-scale modeling approach.

1.4 Motivation

Nowadays, organic electronic device industry is promising because they already replaced and in the near future, will replace their silicon-based analogues. In order to be competitive on the market, compare to the silicon-based devices, high efficiency and stability are indispensable and in order to improve these properties systematically, fundamental understanding physical and chemical process is needed. Specifically, it is important to understand the relation between chemical structure, amorphous morphology and properties of the resulting thin film or device. For the purpose of achieving this understanding, simulation models and methods which can be applicable on different length and time scale should be combined. In this thesis, as mentioned in chapter 1.3.2 we will focus on microscopic and mesoscopic levels of description to simulate charge carrier transport and obtain the charge carrier mobility in amorphous films which consists of small molecules.

1.5 Contents of the thesis

In this chapter, we have discussed the basic concepts of OLEDs, charge transfer theories, brief history of charge transport simulation methodology and the motivation of the research. During this thesis, we will focus on the Multi-scale modeling' methods which is also called 'Microscopic model' to explain the different electrical property between BCP and NBPhen molecule which have similar molecular structure but different mobility value.

In Chapter 2, we will take a closer look on the Microscopic charge transport simulation method from morphology building to solving the master equation using Kinetic Monte Carlo (KMC) method, and finite-size scaling of charge carrier mobility due to its limitations on the simulation length scale.

In Chapter 3, we will focus on understanding the different mobility values between BCP and NBPhen molecule from macroscopic to microscopic point of view.

Finally, we will end the thesis with a summary and conclusion in Chapter 4.

Chapter 2

Microscopic charge transport simulation

2.1 Workflow of Microscopic charge transport simulation

The workflow for microscopic charge-transport simulations is depicted in Fig 2.1. The first step is the generation of an atomistic morphology (sec. 2.2) which consists of force field parametrization, energy minimization for single molecule, construction of initial amorphous system, energy minimization for initial system, and heating and cooling process in NPT ensemble condition. Next, we construct a list of pairs (neighbor list), which reduces the number of calculation for charge transfer rates. After choosing the expression for the charge transfer rate (sec. 2.6), we will calculate reorganization energy (sec 2.3), site energies (sec 2.4) and transfer integrals between neighbor list molecules (sec. 2.5). Combining neighbor list and charge transfer rate, we can construct the system as directed graph and the corresponding master equation can be solved using either numerical method or kinetic Monte Carlo method (sec. 2.7). The latter, kinetic Monte Carlo (KMC) method explicitly simulates the dynamics of charge carriers by

constructing a Markov chain in state space and can find both stationary and transient solutions of the master equation.

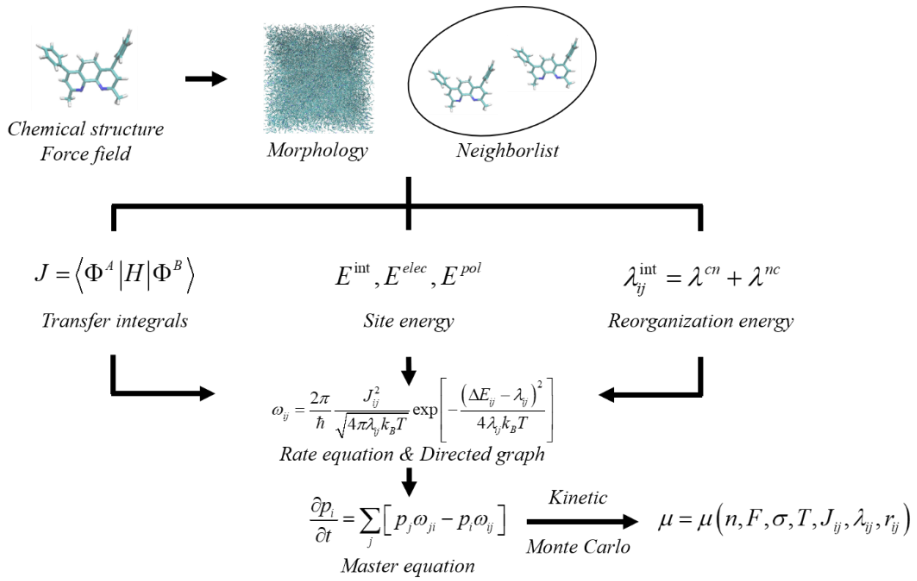

Figure 2.1 Workflow of microscopic simulations of charge transport in organic semiconductors.

2.2 Material morphology

There are several kinds of large-scale morphology of an organic semiconductor: from ultra-pure crystals to totally disordered system. However, there is no generic methodology on how to construct and predict the system. In general, classical molecular dynamics or Monte Carlo methods are used to construct the partially disordered organic semiconductor system. The morphology of such systems has various characteristic time and length scale from ps to several ns range, and for the system which needs far longer time and length scale (μs to ms scale), systematic coarse-graining method[17] can be used to enhance the accuracy of predicting the morphology of thermodynamically equilibrated system. In this thesis, we will use classical molecular dynamics (MD) methods to construct and analyze the amorphous morphology which consists of small molecules.

2.2.1 Force field parametrization

In classical molecular dynamics method, overlapping of electron clouds between molecules can be described as interaction of point masses centered at each atoms via effective potentials. This potential

energy function is composed of several terms representing different types of interaction, and typical form of potential energy can be described as below.

$$U_{tot} = U_{bond} + U_{angle} + U_{dihedral} + U_{vanderWaals} + U_{coulomb}$$

First three terms on the right side are called bonded interactions and the others are called non-bonded terms. Firstly, we will discuss the bonded interactions. U_{bond} refers to the interaction between atoms that are connected covalently. Stretching and contracting a bond makes an increase in potential energy, so for every bonded atoms, near the equilibrated state, the stretching or contracting energy can be approximated with a parabola (harmonic approximation)

$$U_{bond} = \frac{1}{2} k_{bond} \left(x - x_0 \right)^2$$

where k_{bond} corresponds to the force constant (spring constant) determining the strength of the bond, x is the distance between atoms and x_0 is the equilibrium distance. U_{angle} means the potential energy

value with changing angle formed among three bonded atoms. This also can be approximated with a parabola as the bonded interaction does.

$$U_{angle} = \frac{1}{2} k_{angle} \left(\theta - \theta_0 \right)^2$$

where k_{angle} corresponds to the force constant (spring constant) determining the strength of the bond, θ is the angle between three atoms and θ_0 is the equilibrium angle.

Particularly, with respect to dihedral potential, we can divide this term into two categories: proper dihedral type and improper dihedral type. For proper dihedral type, when a molecule has a central bond between two atoms and they are bonded to the opposite side of this bond, twisting these two atoms around the central single bond causes a change in potential energy. The potential for this contribution is calculated by a 'Ryckaert-Bellemans (RB) function'

$$U_{prop.dihedral} \left(\psi \right) = \sum_{n=0}^{5} V_n \cos^n \psi$$

where ψ is the dihedral angle and $C_0 - C_5$ are six coefficients defined in the force field for each dihedral. These coefficients were taken from the existing force field (e.g. OPLS-AA force field[18]), but new coefficients for the dihedral between residues of the molecule should be parametrized with reference to the DFT results. In the next paragraph, we will discuss how to reparametrize the RB coefficients in detail[19] and its workflow is illustrated in a flow chart in Figure 2.2.

First, we freeze the middle dihedral angle between specific residues using dihedral constraints, and then optimize the geometry of the molecule with DFT method. Then, the total energies of each frozen dihedral structures are compared to the structure with the lowest energy of the molecule. The six RB coefficients are set to zero at the first time of the energy minimization calculations. After this step, energy minimization calculation is performed on the same frozen dihedral angle structures as in DFT. And the energies of these are compared with reference to that of DFT calculation.

The purpose of this procedure is that if we have the ideal RB coefficients for the dihedral angle, the potential energy profile from the MD simulation will be the same with that of DFT calculation which means

that the difference between the energies ΔE_{ψ} with each dihedral angle is zero.

To verify the accuracy of the RB coefficients, we calculate the sum of the squared deviations S between ΔE_{ψ} and $U_{RB}(\psi)$. The value of the summation can be minimized by changing RB coefficient for every iteration step until we get the lowest possible value for the sum of the squared deviations.

$$S = \sum_{-180}^{180} \left(\Delta E_{\psi} - E_{RB}(\psi) \right)^2$$

Next, for the improper dihedral type, we can assume a special case when all the four atoms forming the dihedral constitute a planar structure. They are usually used to keep the planar structures of aromatic rings, their substituents and also to preserve the chirality of the molecules. Improper dihedral can be approximated as a harmonic potential according to the equation

$$U_{improp.dihedral} = \frac{1}{2} k_{improp} \left(\xi - \xi_0 \right)^2$$

where k_{improp} is the improper dihedral force constant, ξ the improper dihedral angle between the four atoms and ξ_0 the reference value for the improper dihedral angle.

Next, we will discuss the non-bonded interaction terms for two atoms that are not covalently connected but within a certain cut-off distance of each other. These consist of electrostatic coulomb potential $U_{coulomb}$ and van der Waals potential $U_{vanderWaals}$. First, the coulomb interactions between two charged atoms i and j is calculated by

$$U_{coulomb} = \frac{1}{4\pi\varepsilon_0\varepsilon_r}\frac{q_i q_j}{r_{ij}}$$

where q_i and q_j are the partial charges of atoms i and j, ε_0 the vacuum permittivity, ε_r the relative permittivity and r_{ij} the distance between the two atoms. Next, the van der Waals interaction between atoms can be calculated by using Lennard-Jones potential that is used to consider non-electrostatic interactions which contain a short-range

repulsion term and a long-range attraction term between two atoms. Similar to the coulomb potential, the Lennard-Jones potential is inversely proportional to the distance between atoms r_{ij} and it is given by the equation

$$U_{vanderWaals} = 4\varepsilon_{ij}\left(\left(\frac{\sigma_{ij}}{r_{ij}}\right)^{12} - \left(\frac{\sigma_{ij}}{r_{ij}}\right)^{6}\right)$$

where ε_{ij} and σ_{ij} are parameters defined for two atoms where the interaction is being calculated. Specifically, in the OPLS-AA force field, they are defined according to equations

$$\varepsilon_{ij} = \left(\varepsilon_{ii}\varepsilon_{jj}\right)^{1/2}, \quad \sigma_{ij} = \left(\sigma_{ii}\sigma_{jj}\right)^{1/2}$$

where ε_{ii}, ε_{jj} corresponds to ε parameters defined in the force field for atoms i and j and σ_{ii}, σ_{jj} correspond to σ parameters defined in the force field for atoms i and j respectively.

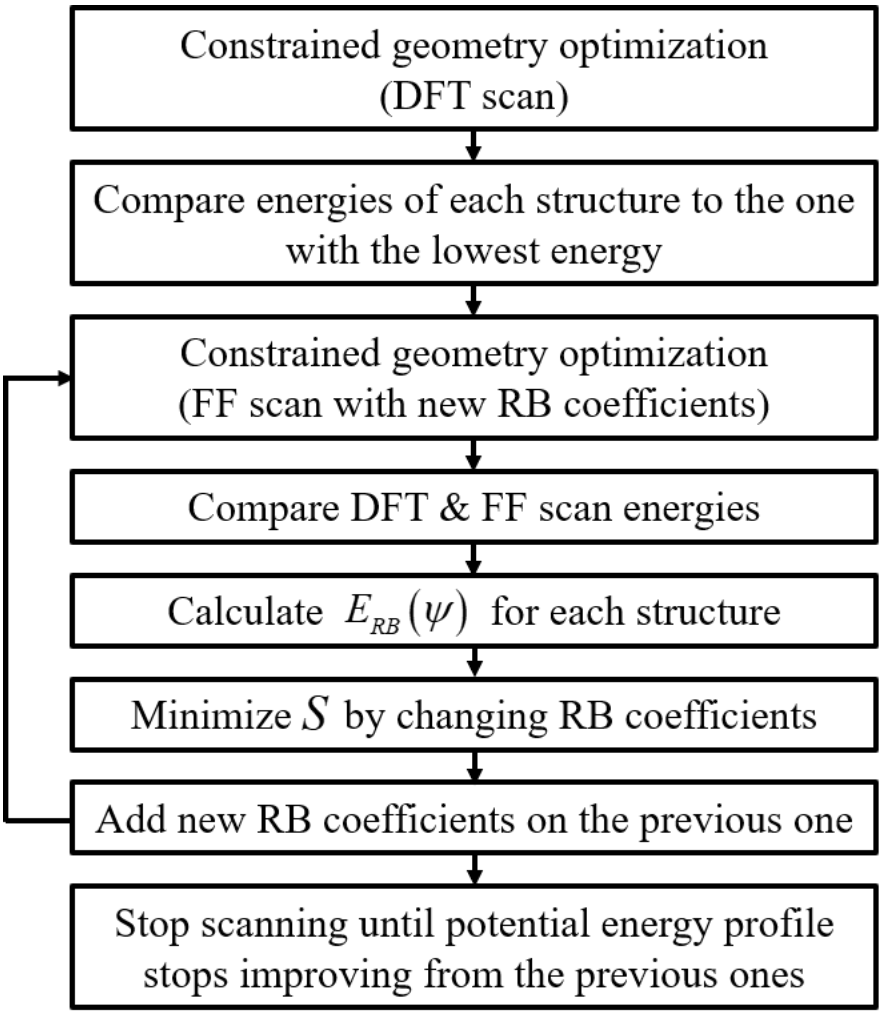

Figure 2.2 Workflow of parametrizing Ryckaert-Bellemans coefficients for proper dihedral potential equation.

2.2.2 Constructing initial amorphous system

With the parametrized force field at hand, we can generate the initial amorphous system for specific molecule. First, specific type of molecule is randomly distributed in a simulation box using the PACKMOL[20] package. Next, as molecular dynamics force-field contain repulsive terms that increase abruptly as the atom-to-atom distance becomes shorten, the distance between atoms from different molecules must be large enough so that repulsive potentials do not disrupt the simulations. Frequently, the instability and non-differentiability of the potential energy term resulting from overlapping between atoms is hard to overcome. Consequently, we execute energy minimization step for initial system which is made from PACKMOL package.

The algorithm used in this step to minimize the energy of initial structure is the 'steepest descent algorithm'

$$r_{n+1} = r_n - \lambda_n \nabla U\left(r_n\right)$$

where r_n is the position vector of nth step, λ_n is the … parameter which can determine the accuracy and efficiency on finding local

minimum energy position. The idea of this method is to calculate the derivative of potential energy function with respect to position vector r and follow the direction of the negative gradient, which corresponds to the same direction as that of driving force. The nearest local minimum position from the initial position can be found by moving along the greatest local gradient of the potential energy function.

2.2.3 Heating and Cooling process

After the initial amorphous system is energy minimized, we move on to the next step of successive heating and cooling process of amorphous system in NPT ensemble condition.

First, we anneal the system from 300K to the temperature which is larger than the glass transition temperature, and next we quench the system to the room temperature (300K) condition. All MD simulations are performed in the NPT ensemble condition using canonical velocity rescaling thermostat[21], and Berendsen barostat[22] for pressure coupling, and Ewald technique for long-range electrostatic interaction.

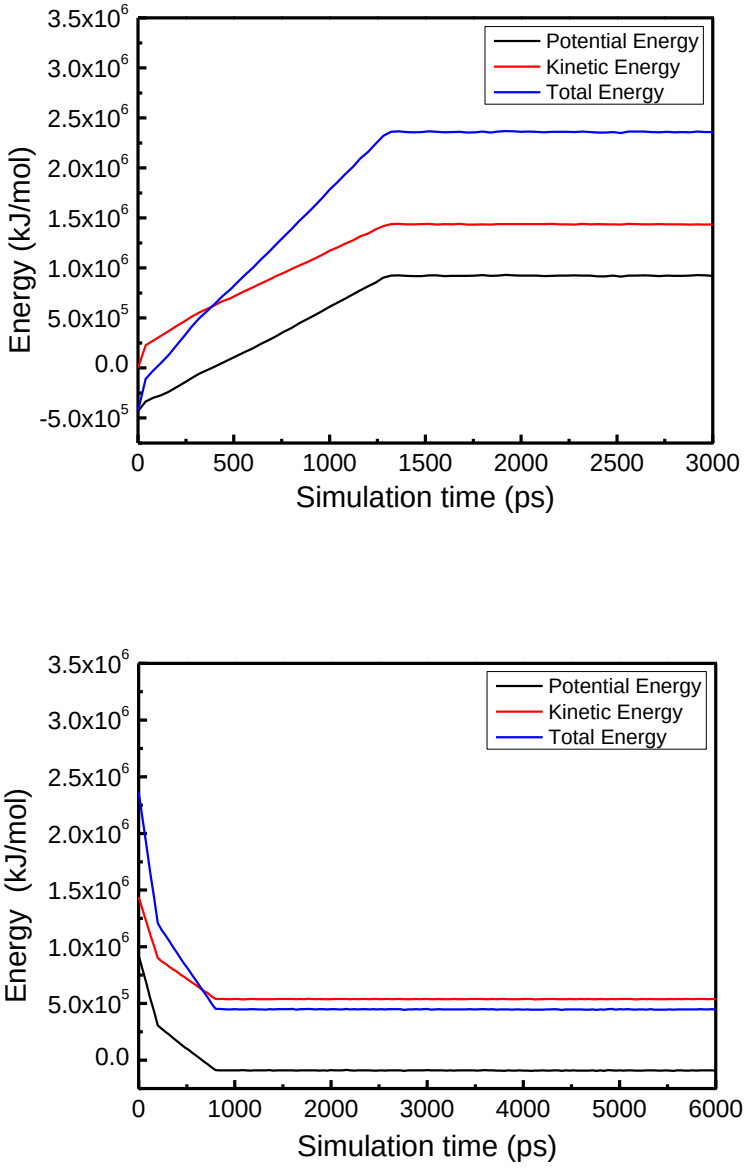

Figure 2.3 Energy diagram of heating (annealing) and cooling (quenching) process on amorphous system

2.3 Reorganization energy

In Marcus theory, reorganization energy λ_{ij} considers the change in nuclear degrees of freedom as the charge (electron or hole) moves within the charge transfer complex from donor i to acceptor j. A depiction of the classical harmonic approximation of the charge transfer is shown in Fig 2.4. In this figure, the donor that has charge carrier (charged or excited) has a potential energy curve that is displaced with respect to the energy curve of the ground state. In the same manner, the potential energy curve for the acceptor ground and charged state are displaced with respect to each other. This displacement causes energy to be lost into vibrational modes of the system in every charge transfer process. This can be seen by the difference in length of the vertical arrows in the figure. It has two contributions: intramolecular, $\lambda_{ij}^{\text{int}}$, which is due to reorganization of nuclear positions of the molecules i and j inside the complex (inner-sphere), and intermolecular (outer-sphere), λ_{ij}^{out}, which is due to the relaxation of environment. In what follows, we will discuss how these two contributions can be calculated.

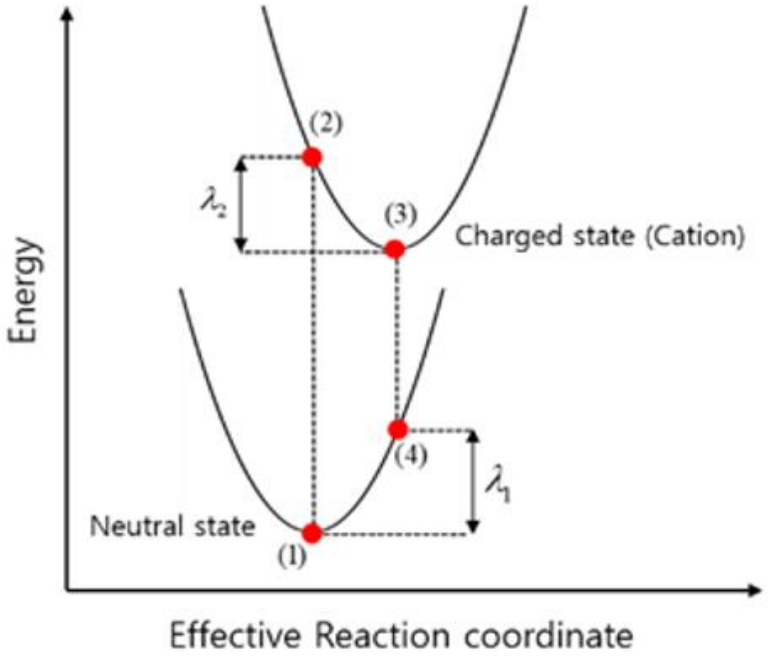

Figure 2.4 Potential energy surface of donor and acceptor in charged and neutral states

2.3.1 Intramolecular reorganization energy

The inner-sphere reorganization energy can be calculated from the potential energy curves using the four point method[23]. In the four point procedure, we use DFT method to calculate the energies at each points indicated in the figure. The first point (Point 1) corresponds to the 'relaxed ground state energy', the second point (Point 2) is the charged state energy in the ground state molecular geometry. The third (Point 3) is the relaxed charged state energy, and the fourth (Point 4) corresponds to the ground state energy in the charged state geometry. Consequently, the reorganization energy is then given by the following equation.

$$\lambda_{ij}^{\text{int}} = \lambda_i^{cn} + \lambda_j^{nc} = \left(U_i^{nC} - U_i^{nN}\right) + \left(U_j^{cN} - U_j^{cC}\right)$$

where U_i^{nC} is the internal energy of the neutral molecule i in the geometry of its charged state (small n denotes the state and capital C the geometry). Similarly, U_j^{cN} is the energy of the charged molecule j in the geometry of its neutral state. We should note that the potential energy surface of the donor and acceptor molecules are not identical for chemically different compounds or conformers of the same molecule. In

other words, $\lambda_i^{cn} \neq \lambda_j^{cn}$ and $\lambda_i^{nc} \neq \lambda_j^{nc}$. Thus, $\lambda_{ij}^{\text{int}}$ is not single molecular property but the property of the charge transfer complex.

2.3.2 Intermolecular reorganization energy

During the charge transfer reaction, molecules outside the charge transfer complex (e.g. solvent molecules) can be reoriented and be polarized in order to adjust for changes in electric potential, resulting in the outer-sphere contribution to the reorganization energy. becomes important if charge transfer reaction occurs in a polarizable environment. The outer-sphere contribution can be computed using the dielectric response function, polarizable force fields, or hybrid quantum mechanics/molecular mechanics methods. However, we can neglect the outer-sphere contribution in this situation.

2.4 Site energy

A charge transfer reaction between molecules and is driven by the site energy difference, $\Delta E_{ij} = E_j - E_i$. Since the transfer hopping rate, ω_{ij} depends exponentially on the site energy difference

$\Delta E_{ij} = E_j - E_i$,computing and analyzing its distribution as accurately as possible is one of the most important procedure in extracting charge carrier mobility in microscopic simulation process. The total site energy difference is influenced by internal energy difference, external applied electric field, electrostatic interactions[24] and polarization effects. Now we will discuss how to estimate these contributions by using first-principles calculations and polarizable force-fields.

2.4.1 Internal energy

The contribution to the site energy difference due to different internal energies can be expressed as describe below.

$$\Delta U_{ij}^{\text{int}} = \Delta U_j - \Delta U_i = \left(U_j^{cC} - U_j^{nN}\right) - \left(U_i^{cC} - U_i^{nN}\right)$$

where $U_i^{cn(\text{CN})}$ is the total internal energy of the molecule i in the charged (neutral) state and geometry. ΔU_i corresponds to the adiabatic ionization potential (or electron affinity) of molecule i . If the system consists only one-component molecule and conformational changes are

negligible, we can set $\Delta U_{ij}^{\text{int}} = 0$, while it is significant for donor-acceptor systems.

2.4.2 External applied electric field

The contribution to the site energy difference due to an external electric field F is given by $\Delta U_{ij}^{ext} = q\vec{F} \cdot \vec{r}_{ij}$ where $q = \pm e$ is the elemental charge and $\vec{r}_{ij}$ is the vector connecting the molecules between i and j. For distances between molecules, which are of the order of several nanometers, and moderate fields of $F < 10^6 V/cm$, its value will always be smaller than $0.1eV$.

2.4.3 Electrostatic interaction energy - GDMA

In order to electrostatic interaction take into account, we represent the charge density of the molecule by choosing multipole expansion site per molecule to reproduce the molecular electrostatic potential (ESP), with a set of multipole moments. And there are a number of strategies to arrive at such a collection of distributed multipoles. In this thesis I used the Gaussian distributed multipole analysis (GDMA)[26] method which is

developed by A. stone, operates directly on the quantum-mechanical density matrix, expanded in terms of Gaussian function.

$$\chi_\alpha = R_{LK}\left(\vec{x}-\vec{s}_\alpha\right)\exp\left[-\xi\left(\vec{x}-\vec{s}_\alpha\right)^2\right]$$

$$\rho\left(\vec{x}\right)=\sum_{\alpha,\beta}\rho_{\alpha\beta}\chi_\alpha\left(\vec{x}-\vec{s}_\alpha\right)\chi_\beta\left(\vec{x}-\vec{s}_\beta\right)$$

The aim is to compute multipole moments according to a distributed fashion which means that if we use the overlap product of two Gaussian basis functions yield itself a Gaussian centered.

One important advantage of GDMA method than fitting algorithms such as CHELPG or Merz-Kollman (MK) is that higher-order moments can be derived without large ambiguity.

2.4.4 Induction energy - Thole model

In this thesis, I used the Thole model[27] in order to take into account induction effect in organic amorphous system. This model is based on a point dipole model, where each atom has its polarizability which can be calculated from a dipole field tensor. The limitation of this approach is

that for atoms closer than a certain distance, their interaction energy diverges, that is why the Thole model modifies the dipole-dipole interaction by using damping factor.

2.5 Transfer integrals

In this thesis, I used the approximate method which is called the Zerner's Intermediate Neglect of Differential Overlap (ZINDO)[28] method. Firstly, the transfer integral J_{ij} entering the marcus hopping rate equation can be defined as below

$$J_{ij} = \left\langle \phi^i \middle| H \middle| \phi^j \right\rangle$$

where ϕ^i and ϕ^j corresponds to the diabatic wave function, localized on molecule i and j respectively. And H corresponds to the Hamiltonian of the donor and acceptor pair (dimer). Diabatic states are approximated by the HOMO of monomer in case of hole transport and LUMO for electron transport which is based on the 'frozen core approximation'. Even though the accuracy and result from this semi-empirical method is slightly different from first principle method, it is

faster than ab initio approach since it can avoid self-consistent calculations on each individual monomer and dimer.

2.6 Charge transfer rate equation

Typical time scales of charge transport in disordered organic semiconductors span several orders of magnitude. Hence, treatment of charge dynamics cannot be achieved by using numerical methods with a fixed time step. Instead of that, the methodology based on charge-transfer rates between localized states has to be employed. Since electronic coupling between neighboring molecular sites is weak in an amorphous morphology, we can assume that charges are localized on entire molecules. Intermolecular charge transfer then occurs between molecule i and j which form the charge transfer complex. In this section, we will discuss the most well-known and frequently used rate-expressions that can descript the charge transport in organic semiconductors.

2.6.1 Miller-Abrahams rate equation

In 1960 Allen Miller and Elihu Abrahams formulated an expression for

impurity hopping in an n-type semiconductor. In their work, rate expressions for charge transfer can be postulated based on intuitive physical considerations, as it has been done in the Gaussian Disorder Model (GDM), where the hopping sites are evenly distributed on a discrete lattice. This leads to a rate that is constant when $\Delta E_{ij} = E_j - E_i < 0$ and is weighted by a Boltzmann factor when $\Delta E_{ij} = E_j - E_i > 0$ for leading to the expression expressed below.

$$\omega_{ij} = \nu_0 \exp\left(-2\gamma_{ij} R_{ij}\right) \begin{cases} \exp\left(-\dfrac{\Delta E_{ij}}{k_B T}\right) & \Delta E_{ij} = E_j - E_i > 0 \\ 1 & \Delta E_{ij} = E_j - E_i < 0 \end{cases}$$

Here ω_{ij} is the rate for charge to be transferred from state i to state j, ν_0 is a pre-factor, called the hopping attempt frequency, which is a material specific rate constant and often fit to reproduce experiments. Continuously, R_{ij} is the distance between localized states, which corresponds to several nanometer scale, γ_{ij} is an inverse localization radius describing the decay of transfer integrals (electronic coupling

elements) J_{ij} with the separation according to $J_{ij}^2 = \exp\left(-2\gamma_{ij}R_{ij}\right)$. Finally, k_B is the Boltzmann's constant, T the temperature, and ΔE_{ij} is the driving force for charge transfer reaction (site-energy difference), so that we introduce energetic penalty factor when a hop uphill occurs. The theory should be interpreted as semi-empirical because the thermally activated hopping process does not occur by just single vibration.

Generally, Miller-Abrahams rate equation is used in GDM to understand the qualitative effect of parameters such as the width of the site energy distribution (energetic disorder, diagonal disorder) or disorder in electronic coupling elements (positional disorder, off-diagonal disorder) on the mobility. In order to verify this relation, charge transport is simulated for single carrier type (hole or electron only) on the discrete lattice with site energies randomly withdrawn from a Gaussian distribution of width $\overline{\sigma}$ ($=\sigma / k_B T$). Transfer integrals are described by two site-specific contributions $\gamma_{ij} = \gamma_i + \gamma_j$ each varying randomly according to a Gaussian distribution of width $\overline{\sigma}_\gamma$ so that the variance of the transfer integral is $\Sigma = \sqrt{2}\overline{\sigma}_\gamma$. These allow to derive an empirical

equation for the mobility [??] given by

$$\mu(F,T) = \mu_0 \exp\left[-\left(\frac{2\bar{\sigma}}{3k_B T} \right)^2 + \mathrm{C}\left\{ \left(\frac{\bar{\sigma}}{k_B T} \right)^2 - \Sigma^2 \right\} \sqrt{F} \right]$$

μ_0 and C are fitting constants and F is the electric field. Comparing the mobility values as a function of field and temperature for various combinations of the parameters $\nu_0, \bar{\sigma}, \Sigma$ to experimental value allows one to determine the diagonal and off-diagonal disorder in organic semiconductors.

2.6.2 Marcus rate equation

The simplest and most well-known expression for a charge transport rate which takes into account energetic landscape, polaronic effects, and electronic coupling elements, is the semi-classical Marcus rate[29] equation

$$\omega_{ij} = \frac{2\pi}{\hbar} \frac{J_{ij}^2}{\sqrt{4\pi\lambda_{ij} k_B T}} \exp\left[-\frac{\left(\Delta E_{ij} - \lambda_{ij}\right)^2}{4\lambda_{ij} k_B T} \right]$$

In this equation, rate parameters are $\Delta E_{ij} = E_j - E_i$, the site energy difference (driving force) where E_i is site energy of molecule i, and J_{ij}, the electronic coupling element, which describes the strength of the electronic coupling between two localized (diabatic) states. An additional parameter in the Marcus rate equation is the reorganization energy λ_{ij} that accounts for relaxation of nuclear coordinates after charge transfer. To be specific, it has two contributions $\lambda_{ij} = \lambda_{ij}^{\text{int}} + \lambda_{ij}^{out}$ from degree of freedom inside the charge transfer complex which consists of state i and j (intramolecular reorganization of donor and acceptor) and from outside (outer-sphere reorganization of charge transfer complex and surrounding solvent molecules).

2.7 Solving the master equation; KMC method

After determining the neighbor list between molecules (hopping sites) and charge hopping rates between them, we can solve the master equation, which describes the time evolution of the given system

$$\frac{\partial P_\alpha}{\partial t} = \sum_\beta P_\beta \Omega_{\beta\alpha} - \sum_\beta P_\alpha \Omega_{\alpha\beta}$$

where P_α is the probability of the given system to be in a state α at time t and $\Omega_{\alpha\beta}$ denotes the transition rate from state α to state β. Instead of solving the master equation by iterative numerical method, we can obtain the solution of the master equation by using Kinetic Monte Carlo (KMC) methods. KMC method explicitly simulates the dynamics of charge carriers by constructing a Markov chain system in state space and can get both stationary and transient solutions of the master equation.

In this thesis, we use combined methodology between First Reaction Method (FRM)[30] and Variable Step Size Method (VSSM)[31]. Given the hopping rates, the KMC algorithm is straightforward and can be conducted by the following scheme.

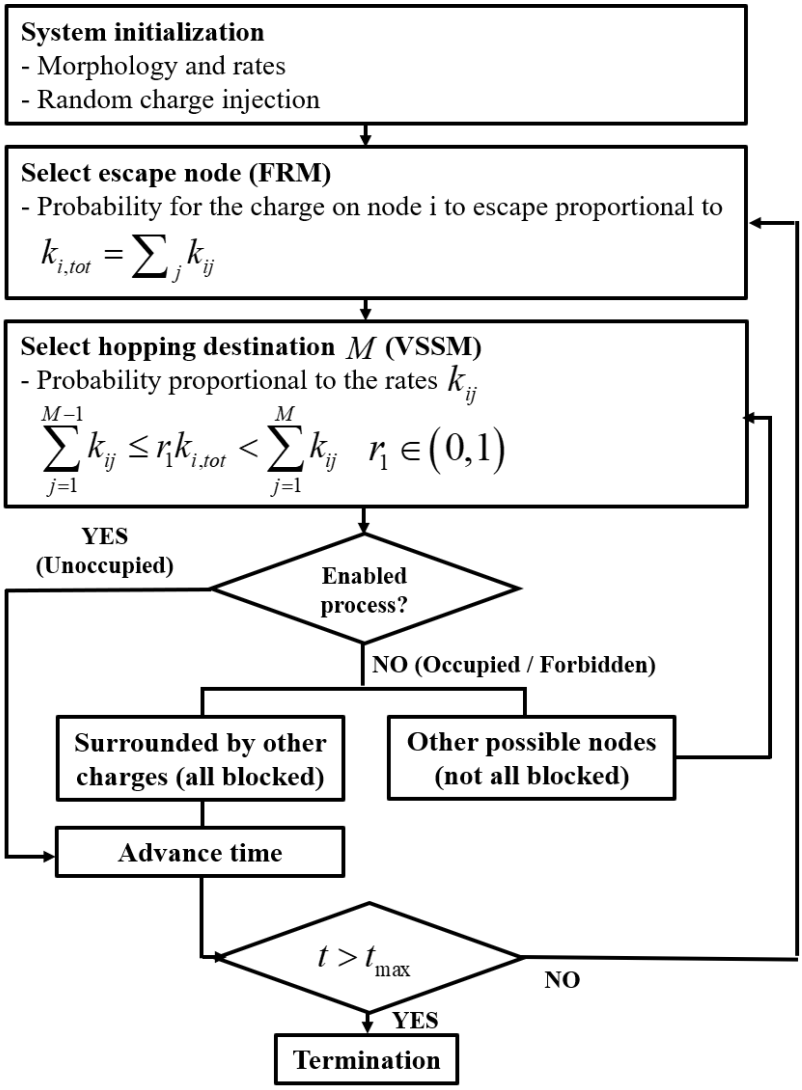

Figure 2.5 Workflow of KMC simulation algorithm. In this thesis, combined methodology between First Reaction Method (FRM) and Variable Step Size Method (VSSM) has been used

Step 1. System initialization

Initialize the KMC system and define all physical parameters that are needed to calculate the hopping rates of all processes. In this stage, termination condition should be defined such as the maximum system time $t_{\max}$ or maximum hopping steps $N_{\max}$, which means that if the system time exceeds maximum system time $t_{\max}$ or the hopping step exceeds the maximum hopping steps $N_{\max}$, the iterative process will be terminated and the simulation will be finished.

Step 2. Select escape node (FRM)

For each charge i, a total escape rate will be calculated as follow

$$k_{i,tot} = \sum_{k} k_{ij}$$

Where the sum is over all neighbors of site i in the neighbor list. At this stage, the disabled process (e.g. if the neighboring site is already occupied with certain type of carrier) do not need to be excluded. After this, a particular charge carrier is selected by using First Reaction Method. In order to do this, waiting time for each charge carrier is

calculated using an evenly distributed random number $r_1 \in (0,1]$. After this, charge i with the smallest waiting time t_i is selected and system time is updated to as follow.

$$t_i = t - t_i^{-1} \ln r_1$$

Step 3. Select hopping destination (VSSM)

After we select which carrier would hop into other site by using First Reaction Method (FRM), we should select a particular site l according to Variable Step Size Method (VSSM) with a probability which fulfills the condition

$$\sum_{j=1}^{l-1} k_{ij} < r_2 \le \sum_{j=1}^{l} k_{ij}$$

where $r_2 \in (0,1]$ is the second random number.

Step 4. Event execution

The presence and positions of the charges and excitons on the lattice are

newly updated according to the selected event. At this stage, we must check whether the selected destination at Step 3 has already been occupied or not. If the destination site is unoccupied, which is enabled process, change the position of carrier. If it is forbidden process, which means that the destination site is occupied, find another possible nodes if the carrier is not all blocked, or if it is surrounded by other charges (all blocked), update the system time.

Step 5. Judgement on termination condition

In KMC simulation, we usually set the terminal condition in two ways; maximum system time $t_{\max}$ or maximum hopping steps $N_{\max}$. If the system does not meet this condition, go back to Step 2 and repeat simulation, and if it meets the condition, the iterative KMC simulation will be terminated.

2.8 Finite-size scaling of charge carrier mobility

In spite of its predictability and prescreening of material candidates which are used in organic semiconductor and organic photovoltaics among large number of molecules, the limit of this approach is the computationally demanding calculation of hopping rates for every pair of neighboring molecules, in particular, intermolecular transfer integral values. Due to its computational cost, employing DFT method and Molecular Dynamics simulation method can handle the system of up to several thousand molecules. Consequently, simulated system only covers several nano-meter thick and, if high energetic disorder exists, charge transport becomes dispersive at room temperature. This makes the measured mobility values from simulation be system-size dependent which cannot be the representative mobility value of certain molecule in ambient condition. In simulations, the dimension of the box ranges from 1~10nm scale and often duplicated in the direction of the field before the charge dynamics is simulated by introducing periodic boundary condition. However, it is nothing more than duplicating the simulation box in certain direction which cannot solve dispersive transient in small system. Thus, in order to extract nondispersive charge carrier mobility from simulations of small systems, alternative methods should be

applied.

Analysis of dependencies between E_N / σ and number of sites (N) or $\sigma / k_B T$ yields an empirical expression for the transition point between the dispersive and nondispersive transport region, for large N,

$$\left(\sigma / k_B T\right)^2 = -5.7 + 1.05 \ln N$$

In the case of Marcus rates, the temperature dependence of the nondispersive mobility at zero field reads

$$\mu(T) = \frac{\mu_0}{T^{3/2}} \exp\left[-\left(\frac{a}{T}\right)^2 - \left(\frac{b}{T}\right) \right]$$

where a, b, and μ_0 are material constants.

In case of hole transport in BCP, where sigma = 0.138eV, it is estimated that the non-dispersive region is generated for temperatures above critical temperature Tc = 973K for the simulation box we considered (N

= 3000 molecules). This means that when KMC simulation is executed at room temperature condition, the mobility might be dispersive. In this case, we can obtain the non-dispersive mobility by using the temperature-based extrapolation technique[32,33].

Chapter 3

Application: Understanding mobility difference between BCP and NBPhen molecule

3.1 Introduction

In chapter 2, we constructed the amorphous morphology, calculated electronic properties of molecules such as site energies, transfer integral and reorganization energy, and finally executed Kinetic Monte Carlo simulation to explicitly simulate the charge dynamics of electron or hole. Now we are going to analyze the results of the microscopic simulation and find out the reason why the mobility value of electron and hole for BCP and NBPhen is different from each other in a microscopic and macroscopic manner.

3.2 Simulation results and analysis

First, in Figure 3.1 and Figure 3.2, we can see the temperature dependent mobility of electron and hole for BCP and NBPhen molecule respectively.

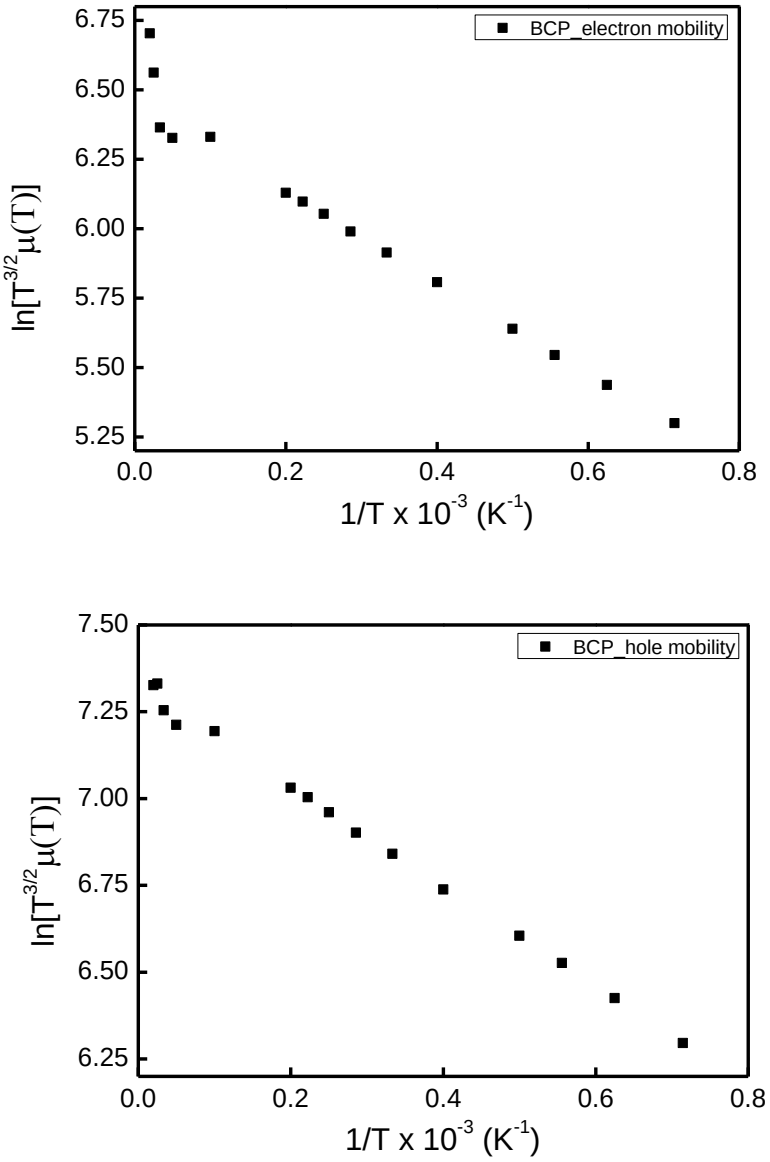

Figure 3.1 Temperature dependent mobility of BCP molecule

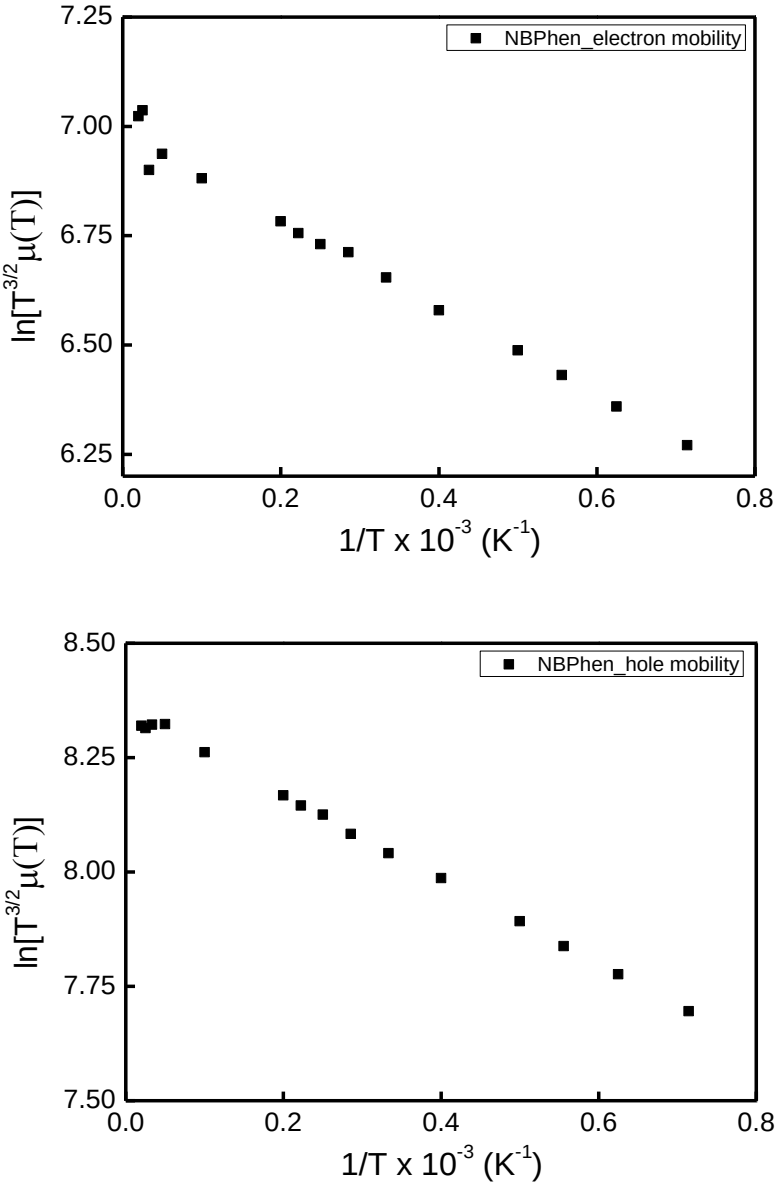

Figure 3.2 Temperature dependent mobility of NBPhen molecule

In order to extract non-dispersive mobility of each molecule, we executed curve fitting to the simulation results, and the fitting equation, its parameters, and extracted non-dispersive mobility of each molecule are described below.

	BCP		**NBPhen**	
	electron	**Hole**	**electron**	**hole**
μ_0	628.673	1487.287	1070.160	4229.293
a	-299.513	260.809	251.849	-126.426
b	1551.265	1365.204	941.675	905.460

Table 3.1 Extracted fitting parameters and non-dispersive electron / hole mobility of BCP and NBPhen molecular system

We can see that the simulated charge carrier mobility of NBPhen is 17 times larger and 23 times larger than that of BCP, where the experimentally measured electron mobility of NBPhen is also 9 times larger than that of BCP. In this chapter, we are going to unveil the reason of difference in mobility between BCP and NBPhen by analyzing three

factors: Molecular dipole distribution, Reorganization energy, and Transfer integral value.

3.2.1 Molecular dipole distribution

In order to analyze the effect of energetic disorder, we can compare the values of ground state dipole moment of single molecule[34,35,36] (Table 3.2) and molecular dipole distribution in amorphous system. From the result of fast quenching process in MD simulation, we can extract the molecular dipole distribution of BCP and NBPhen respectively, and the results are shown in the next page (Figure 3.3).

System	$\mu(D)$	σ_{hole}	$\sigma_{electron}$
BCP	2.880	0.138	0.144
NBPhen	3.240	0.199	0.203

Table 3.2 Single molecular dipole moment and energetic disorder of BCP and NBPhen amorphous system

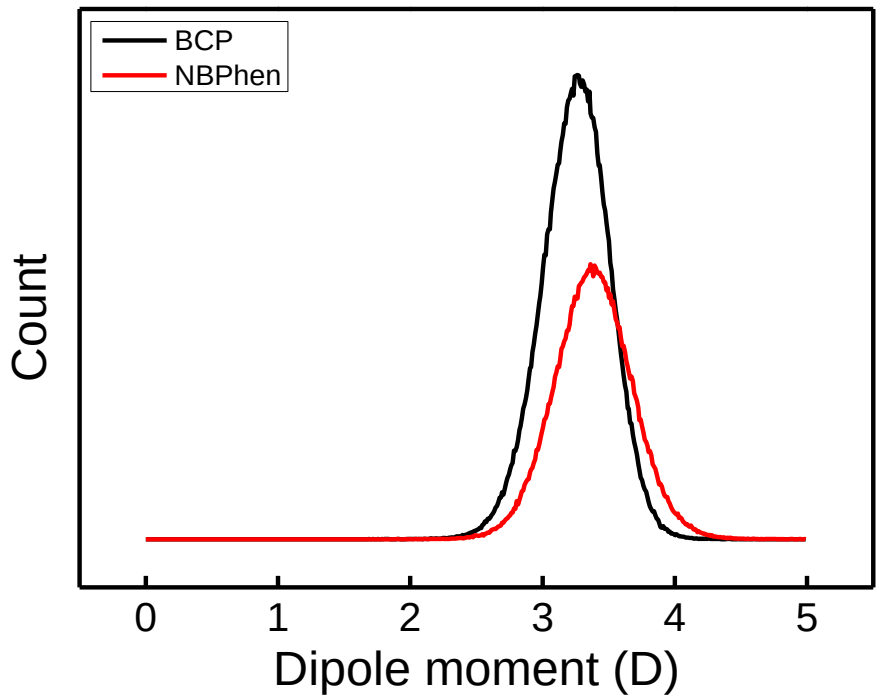

Figure 3.3 Molecular dipole distribution of BCP and NBPhen molecular system

There are several reasons of fluctuation on molecular dipole moment: rotation of single bonds, bending motion and oscillation of covalent bond. For both BCP and NBPhen, dipole moment values of ground state single molecule are 2.880D and 3.240D respectively, which are quite large. However, not only the ground state dipole moment value but also the fluctuations in dipole moment is important factor that affects energetic disorder. Presence of such a large fluctuations in dipole moments within a simulation box induces local electric field which can interact with the charge carrier leading to relatively large energetic disorder (Figure 3.4). When we compare the distribution of dipole moment of BCP and NBPhen, the distribution is broader for NBPhen than that of BCP, which results in larger energetic disorder value. In this analysis, it seems that the mobility of NBPhen would be smaller than BCP because the typical relation between mobility and width of the site energy distribution (energetic disorder) are well known as described below.

$$\mu \propto \exp\left[-C\left(\frac{\sigma}{k_B T}\right)^2\right]$$

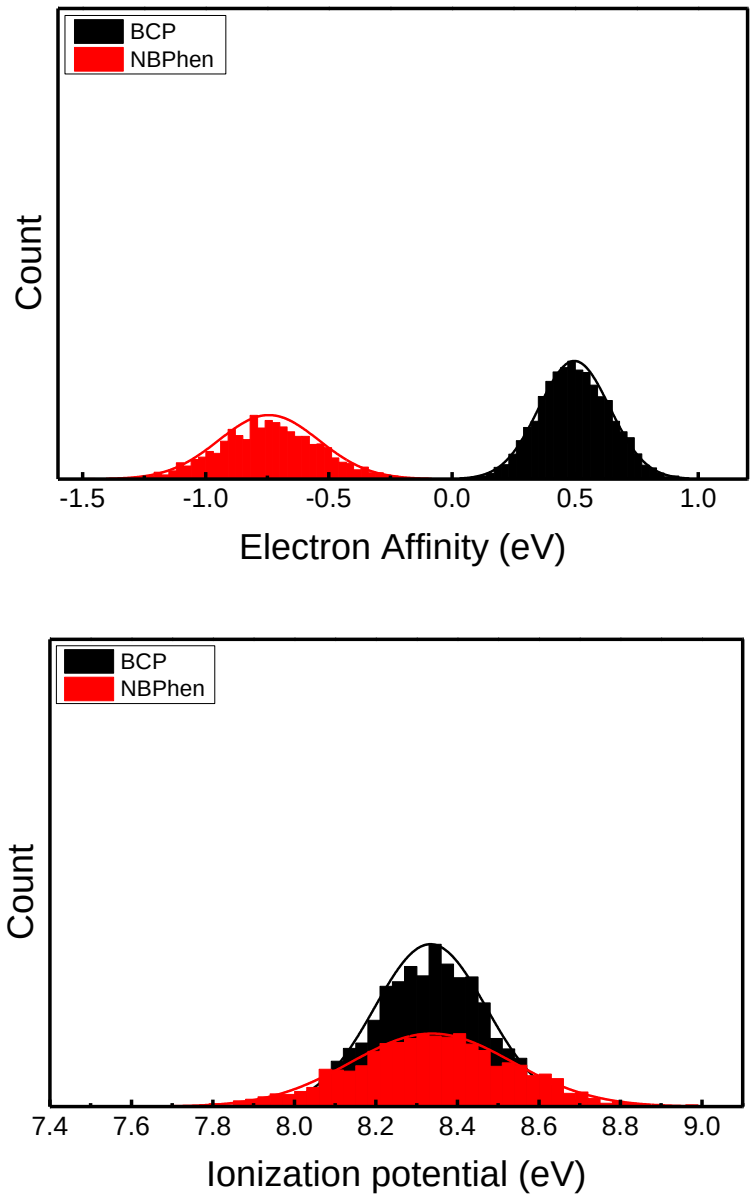

Figure 3.4 Density of states (DOS) of BCP and NBPhen system

3.2.2 Reorganization energy

By using four point method, we can calculate the internal reorganization energy of each molecule in the vacuum environment. In this simulation, I executed the DFT calculation using m062X functional and 6-31g(d,p) basis set and the calculation result is written below (Table 3.3).

System	Hole (eV)	Electron (eV)
BCP	0.4923	0.5528
NBPhen	0.3183	0.3447

Table 3.3 Internal reorganization energy of BCP and NBPhen.

We can find that the reorganization energy of NBPhen is smaller than that of BCP which makes NBPhen more advantageous in obtaining higher hopping rate. At this point, we can make a decision on why the internal reorganization energy of NBPhen is smaller than that of BCP. For NBPhen, the two substituent naphthalene groups make NBPhen

molecule have longer conjugation length and larger conjugated core size that results in cost less energy dissipation when the charge carrier moves between donor and acceptor.

3.2.3 Transfer integral value

In this part, we can obtain the transfer integral value for all neighbor list pairs by using semi-empirical ZINDO method and their distribution. The distribution is plotted as below in Figure 3.5. In this figure, we can get the average transfer integral value of each type of molecule and carrier type. (Table 3.4)

System	Hole	Electron
BCP	6.35e-5	1.42e-4
NBPhen	9.59e-5	1.61e-4

Table 3.4 Average transfer integral value of BCP and NBPhen for each type of carriers

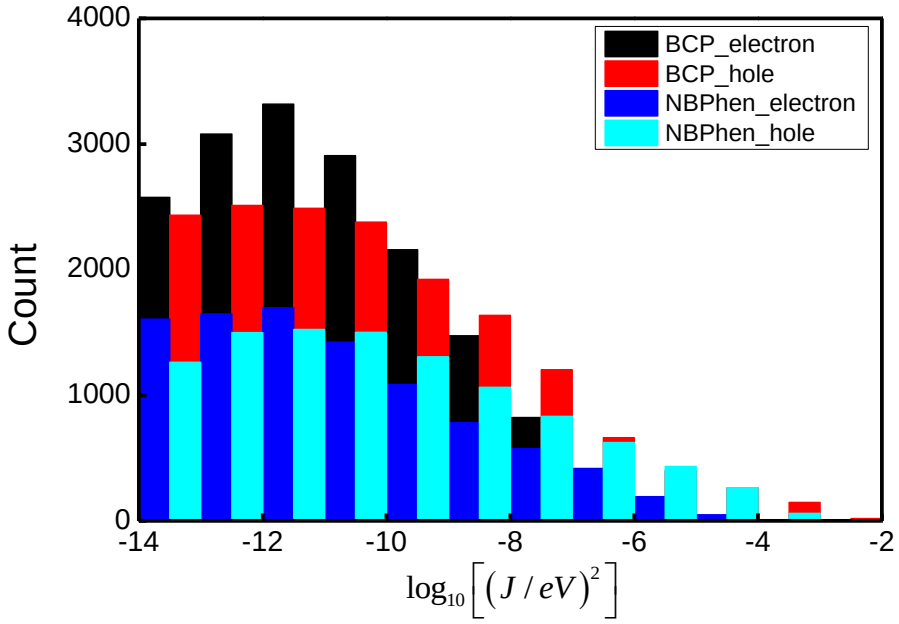

Figure 3.5 Transfer integral distribution of BCP and NBPhen system

As can been seen in the Table 3.4, the average transfer integral value of NBPhen is bigger than that of BCP and the reason of this phenomenon can be analyzed by examining iso-surface of frontier orbital of each molecule (Figure 3.6) and radial distribution function[37] of center of mass of molecules (Figure 3.7) evaluated in atomistic scope.

	Total COM (nm)	Core PHN (nm)	Benzene (nm)	Sub (nm)
BCP	0.431	0.431	0.598	0.406 (Met)
NBPhen	0.484	0.414	0.564	0.666 (Benzene)

Table 3.5 Peak position of radial distribution function of BCP and NBPhen molecular system

As can be seen in Figure 3.6, the HOMO and LUMO of BCP are uniformly distributed over the periphery of the molecule. On the other hand, such an uniform distribution of frontier orbitals are missed in NBPhen molecule, which means that the HOMO and LUMO are found to be rather localized on the core part. With this distribution of frontier orbitals at hand, we will analyze the radial distribution function. In Figure 3.7, the onsets and positions of the peak represents the distance

between center of mass of reference residues, and there are 6 kinds of radial distribution function. From Table 3.5, we see that the distance between the center of mass of entire molecule for NBPhen is larger than that of BCP, that we can predict that the average distance between molecules of NBPhen will be larger than BCP. However, charge carriers do not only occur between the center of mass of entire molecule, but also between the specific residues. Therefore, we should also check the distance between other parts of the residue (e.g. between benzene substituents, benzene ring and phenanthroline, naphthalene substituents etc.). From Table 3.5, we can see that the distance between core phenanthroline residues and benzene substituents for NBPhen are shorter than that of BCP which boosts the transfer integral value because transfer integral value has exponential proportionality to the distance.

To sum up, when energetic disorder, reorganization energy, and transfer integral terms are put together, we can get the hopping rate distribution which is shown in Figure 3.8. It shows that the average value of hopping rate for NBPhen is bigger than that of BCP.

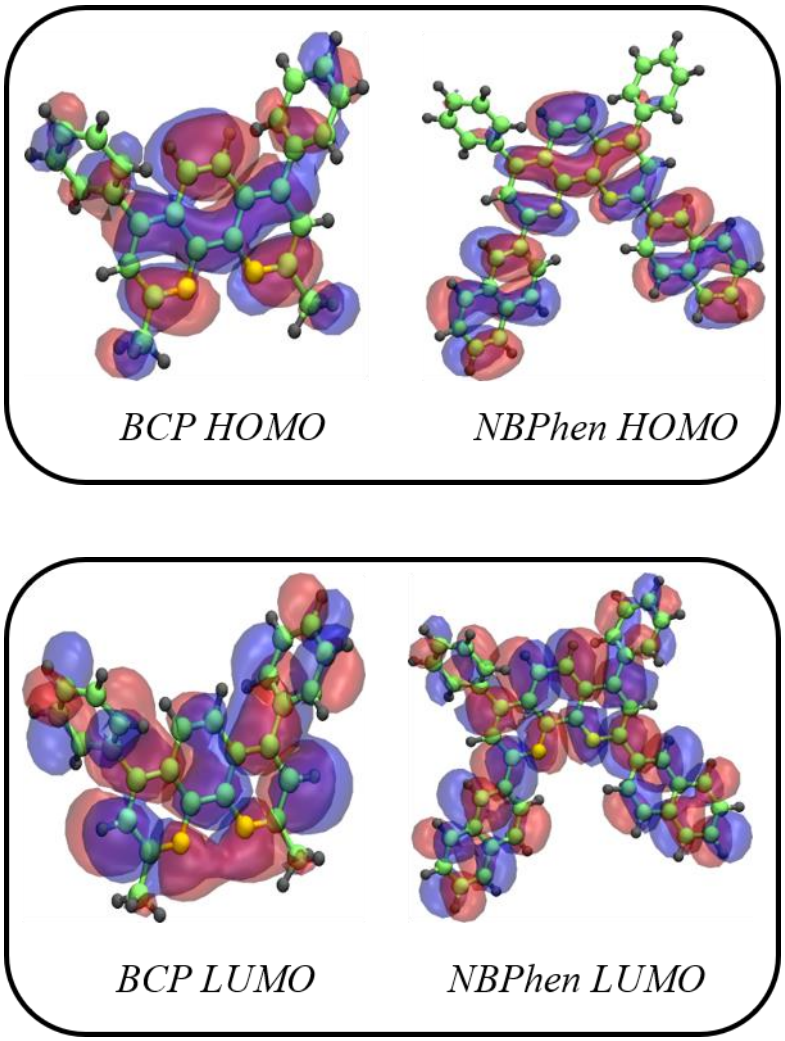

Figure 3.6 Isosurface of the frontier orbital of BCP and NBPhen molecule

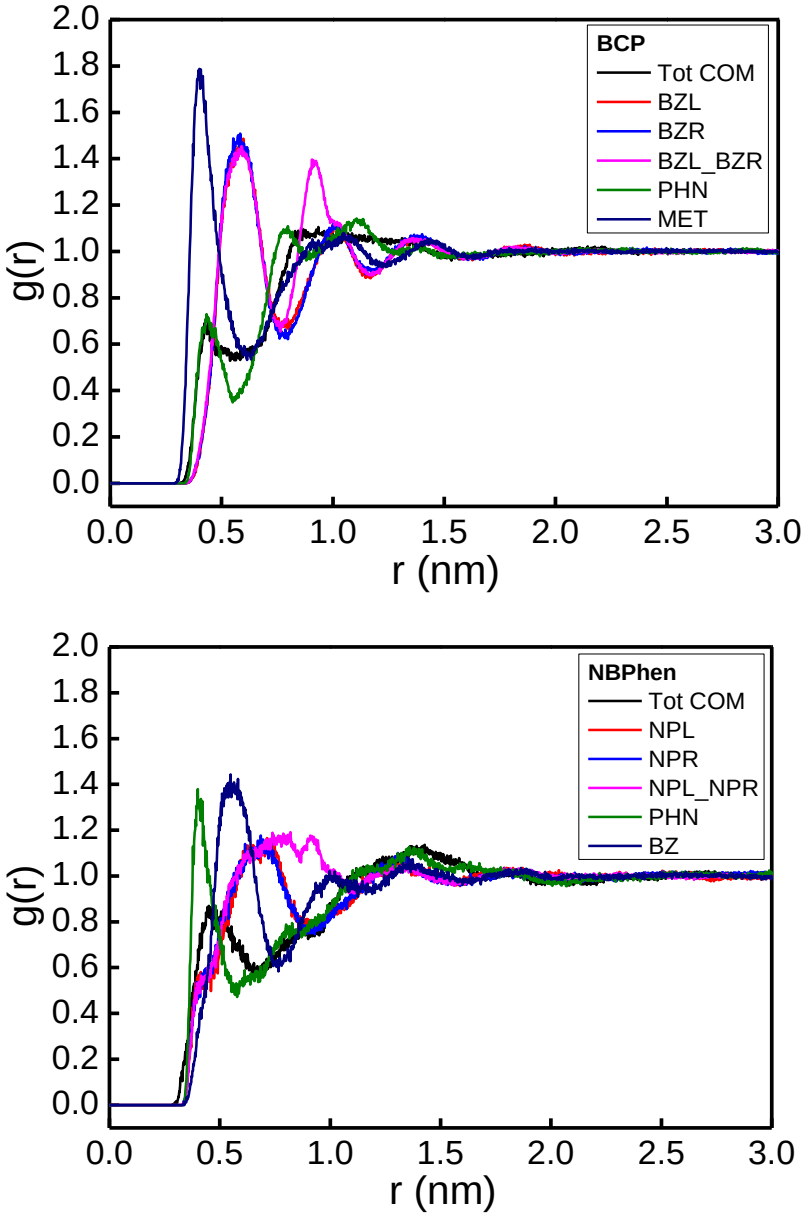

Figure 3.7 Radial distribution function of center of mass of molecules evaluated in atomistic scope

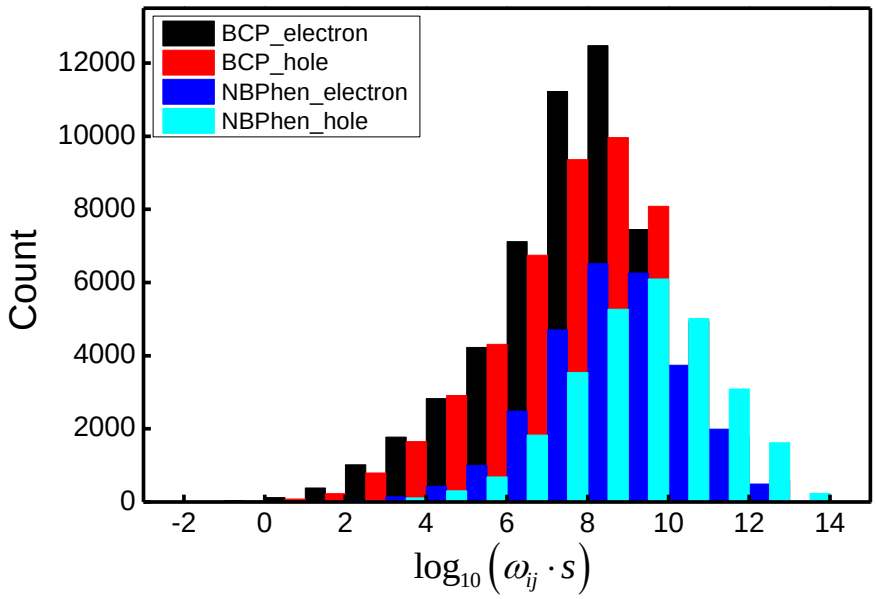

Figure 3.8 Hopping rate distribution of BCP and NBPhen system

3.3 Conclusion

In this chapter, we showed that the mobility difference between BCP and NBPhen by using microscopic simulation method comes from three factors: Energetic disorder term, Reorganization energy term, and finally Transfer integral term.

First, in the respective of energetic disorder term, we found that the molecular dipole distribution of NBPhen was slightly bigger than that of BCP which results in bigger energetic disorder term. In this case, the reason why the larger fluctuation in molecular dipole causes bigger energetic disorder is that the large fluctuations in dipole moment induces the local electric field which interacts with the charge carrier leading to large energetic disorder. In this part, it seems that the mobility value of NBPhen will be smaller than that of BCP.

Next, in terms of reorganization energy, the reorganization energy of NBPhen during charge carrier transfer between donor and acceptor is smaller than that of BCP which is advantageous for higher hopping rate. The reason is that for NBPhen molecule, the naphthalene substituent group causes larger conjugation length and bigger conjugated core size which decreases the reorganization energy value.

Lastly, we can find that the average value of transfer integral for NBPhen

is bigger than that of BCP molecule. The reason of this result can be found by analyzing the radial distribution function of both molecules. If we compare the peak position, which corresponds to the distance between residues of each molecule, the distance between core phenanthroline residues and benzene substituents of NBPhen is smaller than that of BCP which boosts the transfer integral value which results in larger average value of transfer integral because the transfer integral value has exponential proportionality to the distance.

Chapter 4

Summary and Conclusion

In this thesis, I used the multiscale simulation approach which consists of Molecular Dynamics (MD) simulation, Quantum chemical calculation especially in DFT, and Kinetic Monte Carlo (KMC) method to simulate charge dynamics and obtain the charge carrier mobility value. Furthermore, I analyzed the MD, DFT and KMC simulation results in order to find out the reason why the mobility of BCP and NBPhen molecule are different. This can be summarized into three categories: site energy distribution (energetic disorder), reorganization energy, and transfer integral. And we can conclude that we should design a molecule with smaller reorganization energy and larger transfer integral values, even though we cannot predict the energetic disorder value of the molecule that we are interested in. And in order to adjust the electronic properties of molecule and obtain high charge carrier mobility, changing the type of substituent group which can make molecule have higher transfer integral and lower reorganization energy enables us to achieve our goal.

References

1. S. Scholz, D. Knodakov, B. Lussem, K. Leo, *Chem. Rev.* **115**, 16, 8449 (2015)
2. E.M Conwell, *Phys. Rev.* **103**, 51 (1956)
3. N.F Mott, *J. Phys.* **34**, 1356 (1956)
4. T. Holstein, *Annals of Physics.* **8**, 325 (1959)
5. T. Holstein, *Annals of Physics.* **8**, 343 (1959)
6. A. Miller, E. Abrahams, *Phys. Rev.* **120**, 3, 745 (1960)
7. H. Bassler, *Phys. Status Solidi B.* **175**, 15 (1993)
8. J. Frenkel, *Phys. Rev.* **54**, 647 (1938)
9. Yu.N. Gartstein, E.M. Conwell, *Chemical Physics Letters.* **245**, 351 (1995)
10. W. F. Pasveer, J. Cottaar, C. Tanase, R. Coehoorn, P. A. Bobbert, P. W. M. Blom, D. M. de Leeuw, M. A. J. Michels, *Phys. Rev. Lett.* **94**, 206601 (2005)
11. M. Bouhassoune, S. L. M. van Mensfoort, P. A. Bobbert, R. Coehoorn, *Organic Electronics.* **10**, 437 (2009)
12. T. Neumann, D. Danilov, C. Lennartz, W. Wenzel, *J. Comput. Chem.* **34**, 2716 (2013)
13. V. Ruhle, A. Lukyanov, F. May, M. Schrader, T. Vehoff, J.

Kirkpatrick, B. Baumeier, D. Andrienko, *J. Chem. Theory Comput.* **7**, 3335 (2011)

14. W. Kaiser, J. Popp, M. Rinderle, T. Albes, A. Gagliardi, *Algorithms.* **4**, 37 (2018)
15. Z. G. Yu, D. L. Smith, A. Saxena, R. L. Martin, A. R. Bishop, *Phys. Rev. B.* **63**, 085202 (2001)
16. P. Kordt, J. J. M. van der Holst, M. A. Helwi, W. Kowalsky, F. May, A. Badinski, C. Lennartz, D. Andrienko, *Adv. Funct. Mater.* **25**, 1955 (2015)
17. P. Kordt, O. Stenzel, B. Baumeier, V. Schmidt, D. Andrienko, *J. Chem. Theory Comput.* **10**, 2508 (2014)
18. W. L. Jorgensen, D. S. Maxwell, J. Tirado-Rives, *J. Am. Chem. Soc.* **118**, 45, 11225 (1996)
19. M. Schrader, R. Fitzner, M. Hein, C. Elschner, B. Baumeier, K. Leo, M. Riede, P. Bauerle, D. Andrienko. *J. Am. Chem. Soc.* **134**, 6052 (2012)
20. L. Martinez, R. Andrade, E. G. Birgin, J. M. Martinez, *J. Comput. Chem.* **30**, 13, 2157 (2009)
21. Bussi. G, Donadio. D, Parrinello. M, *J. Chem. Phys.* **126**, 014101 (2007)

22. Berendsen. H. J. C., Postma. J. P. M., van Gunsteren. W. F., DiNola. A., Haak. J. R. *J. Chem Phys.* **81**, 3684 (1984)
23. O. Lopez-Estrada, H. G. Laguna, C. Barrueta-Flores, C. Anador-Bedolla, *ACS Omega.* **3**, 2130 (2018)
24. G. D'Avino, L. Muccioli, F. Castet, C. Poelking, D. Andrienko, Z. G. Soos, J. Cornil, D. Beljonne. *J. Phys Condens. Matter.* **28**, 433002 (2016)
25. G. D'Avino, L. Muccioli, F. Castet, C. Poelking, D. Andrienko, Z. G. Soos, J. Cornil, D. Beljonne. *J. Phys Condens. Matter.* **28**, 433002 (2016)
26. A. J. Stone, *J.Chem. Theory Comput.* **1**, 1128 (2005)
27. B. Thole. *Chemical Physics.* **59**, 341 (1981)
28. J. Kirkpatrick. *International Journal of Quantum Chemistry.* **108**, 51 (2010)
29. Marcus, R. A. *Rev. Mod. Phys.* **65**, 599 (1993)
30. D. T. Gillespie. *J. Phys. Chem.* **81**, 25, 2340 (1977)
31. Bortz, A. B., Kalos, M. H., Lebowitz, J. L. *J. Comput. Phys.* **17**, 10 (1975)
32. A. Lukyanov, D. Andrienko. *Physical Review B.* **82**, 193202 (2010)

33. P. Kordt, O. Stenzel, B. Baumeier, V. Schmidt, D. Andrienko. *J. Chem. Theory Comput.* **19**, 6, 2508 (2014)

34. F. May, M. Al-Helwi, B. Baumeier, W. Kowalsky, E. Fuchs, C. Lennartz, D. Andrienko. *J. Am. Chem. Soc.* **134**, 13818 (2012)

35. M. Schrader, R. Fitzner, M. Hein, C. Elschner, B. Baumeier, K. Leo, M. Riede, P. Bauerle, D. Andrienko. *J. Am. Chem. Soc.* **134**, 6052 (2012)

36. P. Friederich, F. Symalla, V. Meded, T. Neumann, W. Wenzel. *J. Chem. Theory Comput.* **10**, 3720 (2014)

37. N. B. Kotadiya, A. Mondal, S. Xiong, P. W. M. Blom, D. Andrienko, Get-Jan A. H. Wetzelaer. *Adv. Electron. Mater.* **4**, 12, 1800366 (2018)

Curriculum Vitae

Jaeyoung Cho

Department of Materials Science and Engineering

Seoul National University, Seoul, Korea

+82-2-875-2412 (Office)

E-mail: asterisk5758@snu.ac.kr

Education

2018.03 ~ 2020.02 **M.S.**. in Materials Science and Engineering
Supervisor: Professor Jang-Joo Kim
Seoul National University, Seoul, Korea

2015.03 ~ 2018.02 **B.S.** in Chemistry, Materials Science and Engineering
Yonsei University, Seoul, Korea

Research Interests

- Charge transport simulation in Organic semiconductor devices
- Discovering novel materials for energy conversion and storage
- Algorithm design and application of machine-learning methodologies to soft materials

Professional Skills

- Programming skill (C / MATLAB / Python)

- Molecular Dynamics (MD) simulation program (GROMACS)
- DFT calculation program (Gaussian)

Scholarship and Fellowship

- Brain Korea 21 Scholarship (2018.03 ~)
- Honors scholarship, Seoul National University, 2018
- Merit-based scholarship, Seoul National University, 2019

초 록

전자 이동층 물질로 주로 사용되는 BCP와 NBPhen 분자는 서로 다른 전하 mobility 값을 가진다. 구체적으로 실험적으로 측정된 NBPhen의 전자 mobility 값은 BCP의 경우보다 10배 가량 높게 측정되며, 시뮬레이션을 통한 결과에서도 9배 가량 높은 값이 나타났다. 이와 같은 mobility와 분자 구조 사이의 관계를 규명하기 위하여 microscopic simulation 방법론을 사용하였다. 이 방법론에서 유기 박막을 모사한 무정형 시스템을 만들기 위하여 분자 동역학 시뮬레이션 방법이 사용되었으며, 각 분자의 전자 특성 중 transfer integral, site energy, reorganization energy를 구하기 위하여 밀도 범함수 이론과 Polarizable force field 방법론이 사용되었다. 마지막으로 시뮬레이션 상자 안에서 전하의 동역학 특성을 모사하기 위하여 Kinetic Monte Carlo 방법론을 사용하였다. BCP와 NBPhen 사이의 전하 mobility 차이의 원인은 크게 3가지 항목으로 구분할 수 있는데 이는 energetic disorder, transfer integral 그리고 reorganization energy로 구성된다. Energetic disorder의 관점에서는, 상대적으로 더 큰 분자 쌍극자 분포 특성을 갖는 NBPhen의 경우 energetic disorder 값이 크기 때문에 전하 mobility 특성에 음의 효과를 야기한다. 하지만 transfer integral과 reorganization energy의 관점에서는 transfer integral의 평균 값이 크고 reorganization energy 값이 작은

NBPhen이 전하 mobility 값에 있어서 양의 효과를 갖는데, 이는 energetic disorder로부터 야기되는 음의 효과를 뛰어 넘기 때문에 결과적으로 NBPhen의 mobility가 크게 측정되는 것으로 분석 되었다. 본 연구를 통해 Phenanthroline 중심부를 공통으로 가지며 메틸기와 나프탈렌기에서 치환기의 차이점을 갖는 BCP와 NBPhen 분자의 mobility 차이에 대해서만 분석을 하였으나, 이에 더 나아가 다양한 종류의 치환기에 따른 mobility 차이를 통해 일반화가 가능할 것으로 예상되며, 높은 mobility 특성을 갖기 위해서는 낮은 energetic disorder와 reorganization energy 값을 가지며 높은 transfer integral 평균 값을 가지도록 분자를 설계해야 할 것이며, 이는 치환기의 종류에 따른 분자의 전자 구조 차이 분석과 무정형 시스템 내에서의 집합적인 특성 (energetic disorder, transfer integral) 분석을 기반으로 이루어 질 수 있을 것으로 기대된다.

주요어: 전하 mobility, BCP, NBPhen, microscopic simulation, 분자 동역학 시뮬레이션, transfer integral, site energy, reorganization energy, 밀도 범함수 이론, Kinetic Monte Carlo, energetic disorder, 분자 쌍극자 분포
학 번: 2018-27549